Experimental Neurology 320 (2019) 112965

Contents lists available at ScienceDirect

Experimental Neurology

journal homepage: www.elsevier.com/locate/yexnr

Research Paper

LINGO-1 deficiency promotes nerve regeneration through reduction of cell apoptosis, inflammation, and glial scar after spinal cord injury in mice

Li-Jun Huang[a,b,1], Ge Li[a,b,1], Ying Ding[a], Jia-Hui Sun[a,b], Ting-Ting Wu[b], Wei Zhao[a,b], Yuan-Shan Zeng[a,b,c,d,e,*]

[a] Key Laboratory for Stem Cells and Tissue Engineering (Sun Yat-sen University), Ministry of Education, Guangzhou 510080, China
[b] Department of Histology and Embryology, Zhongshan School of Medicine, Sun Yat-sen University, Guangzhou 510080, China
[c] Institute of Spinal Cord Injury, Sun Yat-sen University, Guangzhou 510120, China
[d] Co-innovation Center of Neuroregeneration, Nantong University, Nantong 226001, China
[e] Guangdong Provincial Key Laboratory of Brain Function and Disease, Zhongshan School of Medicine, Sun Yat-sen University, Guangzhou 510080, China

ARTICLE INFO

Keywords:
LINGO-1 knockout
Spinal cord injury
Cell apoptosis
Inflammation
Glial scar
Nerve regeneration

ABSTRACT

Leucine-rich repeat and immunoglobulin domain-containing protein 1 (LINGO-1) is a transmembrane protein that negatively regulates neural regeneration in the central nervous system. LINGO-1 expression is up-regulated after central nerve injury, and is accompanied by cell death. Both LINGO-1 and cell death in the injury microenvironment are thought to limit neural regeneration, but the relationship between LINGO-1 and cell death has not been characterized. To investigate whether *LINGO-1* deletion improves the spinal cord microenvironment after spinal cord injury (SCI) and contributes to cell survival, we generated *LINGO-1* knockout (KO) mice. These mice and wild-type control mice were subjected to spinal cord transection. Fourteen days after spinal cord transection, cell apoptosis, inflammation, glial scar, and growth of nerve fibers were evaluated by immunostaining. The results showed that *LINGO-1* KO mice demonstrated a profound reduction in expression of caspase-3, transferase-mediated deoxyuridine triphosphate biotin nick end labeling (TUNEL), ionized calcium binding adapter molecule 1 (IBA1), glial fibrillary acidic protein (GFAP), and chondroitin sulfate proteoglycans (CSPGs) compared to controls. In contrast, expression of neurofilament (NF) at the SCI site in *LINGO-1* KO mice was markedly increased compared to that in wild-type mice. These results suggested that LINGO-1 plays a critical role in the injury microenvironment in processes such as cell death, inflammatory response, and glial scar formation. Importantly, *LINGO-1* deletion and a positive microenvironment may exert synergistic effects to promote nerve fiber regeneration. Therefore, inhibition of LINGO-1 may be a therapeutic strategy to promote neural regeneration following SCI.

1. Introduction

Spinal cord injury (SCI) typically includes an initial injury and a secondary injury. In the primary injury, red blood cells, myelin, subcellular debris, and necrotic and apoptotic neurons damaged by the traumatic injury are featured prominently in the lesion epicenter, leading to secondary injury (Tran et al., 2018). Secondary injury mainly includes inflammation, extravasation of infiltrating leukocytes, and proliferation and morphological changes in glial cells (Tran et al., 2018). When the spinal cord is injured, apoptotic and necrotic cells

Abbreviation: LINGO-1, leucine-rich repeat and immunoglobulin domain-containing protein; ATP, adenosine triphosphate; ChABC, chondroitinase ABC; CSPGs, chondroitin sulfate proteoglycans; DSBs, double strands breaks; ECL, enhanced chemiluminescence; ESCs, embryonic stem cells; GAG, glycosaminoglycan; GFAP, glial fibrillary acidic protein; HMGB1, high mobility group box-1 protein; IBA1, ionized calcium binding adapter molecule 1; IHC, immunohistochemistry; IPTG, isopropyl β-D-thiogalactoside; KO, knockout; LB, luria-bertani; MS, Multiple sclerosis; NSCs, neuron stem cells; NF, neurofilament; NHEJ, non-homologous end joining; HR, homologous recombination; PVDF, polyvinylidene fluoride; RPTPσ, receptor protein tyrosine phosphatase sigma; SCI, spinal cord injury; SDS-PAGE, sodium dodecylsulfate-polyacrylamide gel electrophoresis; sgRNA, small guide RNA; ssDNA, single-strand DNA; TUNEL, transferase-mediated deoxyuridine triphosphate biotin nick end labeling; WT, wild-type

* Corresponding author at: Department of Histology and Embryology, Zhongshan School of Medicine, Sun Yat-sen University, 74# Zhongshan 2nd Road, Guangzhou 510080, China.
E-mail address: zengysh@mail.sysu.edu.cn (Y.-S. Zeng).
[1] These authors contributed equally to this manuscript.

https://doi.org/10.1016/j.expneurol.2019.112965
Received 26 March 2019; Received in revised form 14 May 2019; Accepted 23 May 2019
Available online 25 May 2019

release large amounts of alarmins such as chromatin-associated proteins (high mobility group box-1 protein, HMGB1), adenosine triphosphate (ATP), histones, S100 (a family of low-molecular-weight proteins), and interleukins, which can initiate a cascade of inflammatory signaling (Bianchi, 2007; Kono and Rock, 2008; Tran et al., 2018). Resident glial cells, including astrocytes, oligodendrocytes, and microglia, respond swiftly to the altered microenvironment (Tran et al., 2018). Reactive astrocytes undergo proliferation and migrate into the lesion site, forming astroglial scars, which are mechanical barriers to axonal regeneration (Losey et al., 2014; Rhodes and Fawcett, 2004; Yiu and He, 2006). Moreover, in the inflammatory environment, reactive astrocytes increase secretion of chondroitin sulfate proteoglycans (CSPGs), which inhibit axon outgrowth (David et al., 2012; McKeon et al., 1991; Ughrin et al., 2003; Yiu and He, 2006), thus creating a chemical barrier (Losey et al., 2014; Yiu and He, 2006). Therefore, astrocytic glial scars created by chronic secondary injury result in inhibition of axonal growth (Tran et al., 2018).

Leucine-rich repeat and immunoglobulin domain-containing protein (LINGO-1) is a member of the LIG gene super-family, a family of type I membrane proteins containing extracellular domains composed of C2 immunoglobulin-like domains and leucine-rich repeats (Meabon et al., 2016). LINGO-1 is abundantly and exclusively expressed in the central nervous system (Carim-Todd et al., 2003). It is a potent negative regulator of neuron and oligodendrocyte survival, axon extension, axon regeneration, oligodendrocyte differentiation, and axonal myelination (Andrews and Fernandez-Enright, 2015). LINGO-1 has been widely studied in multiple sclerosis (MS) and SCI due to its remarkable role in neurite outgrowth, oligodendrocyte differentiation, and myelination (Ji et al., 2006; Mi et al., 2007). A previous study showed that LINGO-1 level rose 14 days after SCI (Foale et al., 2017; Mi et al., 2004), and inhibition of LINGO-1 increased axonal sprouting, and neuronal and oligodendrocyte survival due to inhibition of RhoA activation (Ji et al., 2006). Mi et al. observed a marked increase in myelinated axons within the spinal cords of *LINGO-1* knockout (KO) mice compared to wild-type (WT) mice in an MS model (Mi et al., 2007). Administration of a LINGO-1 antagonist and LINGO-1-Fc antibody resulted in improved functional recovery of rats following SCI. A previous study showed that *LINGO-1* KO mice had a higher percentage of mature oligodendrocytes and earlier appearance of axonal myelination in the central nervous system than WT mice in an MS model (Mi et al., 2007; Mi et al., 2005). Moreover, compared with WT mice, increased survival of dopaminergic neurons was observed in *LINGO-1* KO mice in a Parkinson's disease model (Inoue et al., 2007).

While the role of LINGO-1 in axonal growth and oligodendrocyte maturation has been well characterized, its relationship with the inhibitory microenvironment during pathological conditions, such as complete spinal cord transection injury, has not been evaluated. It is widely accepted that LINGO-1 is a negative regulator of cell survival and nerve regeneration, and a microenvironment enriched in LINGO-1 in injured spinal cord can inhibit cell survival and nerve regeneration. The extent to which *LINGO-1* KO reduces cell apoptosis, improves the spinal cord microenvironment, and promotes nerve regeneration in the SCI site following complete transection remains to be determined.

SCI models can be classified as contusion, compression, distraction, dislocation, transection, and chemical models. They are chosen depending on the study goals, characteristics of the model, and study resources (Cheriyan et al., 2014). Complete transection is easy to perform, and results in a complex pathophysiological cascade that inhibits potential sprouting from spared axons and leads to formation of scar tissue (Cheriyan et al., 2014; Li et al., 2019). Complete transection is usually regarded as the gold standard for evaluation of nerve fiber regeneration in the SCI site (Wu et al., 2013). Therefore, complete transection with evaluation of nerve regeneration, apoptosis, inflammation, and glial scar formation was selected for investigation of the effects of LINGO-1.

In this study, we used CRISPR/Cas9 technology to generate *LINGO-1* KO mice. These mice, and WT control mice, underwent complete spinal cord transection. Fourteen days after spinal cord transection, the number of apoptotic cells was lower in *LINGO-1* KO mice than in WT mice. In addition, we observed lower expression of ionized calcium binding adapter molecule 1 (IBA1), glial fibrillary acidic protein (GFAP), and CSPGs in and around the SCI site in *LINGO-1* KO mice compared with WT mice. Our study suggested that *LINGO-1* KO increased regeneration of nerve fibers in the SCI site through decreased cell apoptosis and improvement of the spinal cord microenvironment, which included attenuation of inflammation and glial scar formation.

2. Materials and methods

2.1. Animals

Healthy C57BL/6J female mice (21–28 days old) were selected as oocyte donors for superovulation, and then were mated to C57BL/6J stud male mice (49–56 days old) and fertilized as zygote donors. CD1 male mice (≥56 days old) with good mating records were selected to undergo vasectomies, and then mated to CD1 female mice (≥42 days old) to produce pseudo-pregnant mice, which were used as embryo recipients. All animals were housed at the Laboratory Animal Center of Sun Yat-sen University, which is fully accredited by the Animal Care and Use Committee of Sun Yat-sen University, and all experiments were performed in accordance with the National Institutes of Health Guide for the Care and Use of Laboratory Animals.

2.2. Construction of the plasmid co-expressing Cas9 and single-guide RNA (sgRNA)

sgRNAs were designed using the online tools (http://crispr.mit.edu/) developed by the Feng Zhang research group and the gRNA with the highest score (score of 95) was chosen for this study. The pX330-U6-Chimeric_BB-CBh-hSpCas9 vector (Addgene plasmid #42230, a gift from Feng Zhang) expressing Cas9 and sgRNA (Cong et al., 2013) was digested with *Bbs*I and dephosphorylated using Antarctic Phosphatase (NEB, UK). The linearized vector was purified using QIAquick Gel Extraction Kit (QIAGEN, USA). To generate the bicistronic vector (pX330-*Cas9-LINGO-1*) expressing Cas9 and sgRNA against *LINGO-1* (Ran et al., 2013), a pair of oligos for targeting *LINGO-1* exon7 (forward: 5′-CACCGCCGCCACAAAGCGTTTGCGG-3′; reverse: 5′-AAACCCGCAAACGCTTTGTGGCGGC-3′) were annealed, phosphorylated, and ligated to linearize the vector. The ligated vectors were transfected into Stbl3 competent bacteria and inoculated on LB agarose plate. Ten colonies were selected for sequencing analysis to confirm successful ligation of the oligos and the pX330 plasmid. The forward sequence primer was GAGGGCCTATTTCCCATGATT. The successfully ligated clone was amplified for large plasmid yield and extracted using the EndoFree Plasmid Maxi Kit (QIAGEN, USA).

2.3. Primary culture of mouse neural stem cells (NSCs)

Cultured neural stem cells were obtained from the hippocampal tissue of C57BL/6 J mice according to a previously published procedure (Zeng et al., 2005). Briefly, 1–3-day-old mice were anesthetized and the hippocampus was dissociated in cold D-Hank's solution. The suspension was centrifuged at 1000 rpm for 5 min and the cell pellet was resuspended in basal medium (Zeng et al., 2005). The NSCs were cultured at 37 °C in a 5% CO_2 incubator.

2.4. Activity of the pX330-Cas9-LINGO-1 plasmid

After NSCs were cultured for 5–7 days, they were transfected with 800 ng pX330-*Cas9-LINGO-1* plasmid and 800 ng pX330 plasmid (negative control) for 48 h using Nucleofector Kit and 4D-Nucleofector (Lonza, Germany) following the manufacturer's protocol. The genomic

region surrounding the CRISPR target for *LINGO-1* was amplified by PCR using the One Taq DNA Polymerase kit (NEB, USA) according to the manufacturer's instructions. The forward primer was: 5′- TGAACC CTAAAGGAGATGGCACTG-3′, and the reverse primer was: 5′-GTTCTC ACTGATGTCCAGCTTGG-3′. The PCR program was as follows: 95 °C for 3 min; 94 °C for 30 s, 55 °C for 30 s, 72 °C for 1 min, for 35 cycles, then 72 °C for 10 min. The PCR products were sequenced to detect genome modification.

2.5. Production of LINGO-1 sgRNA

To obtain *LINGO-1* sgRNA for microinjection, T7 promoter was

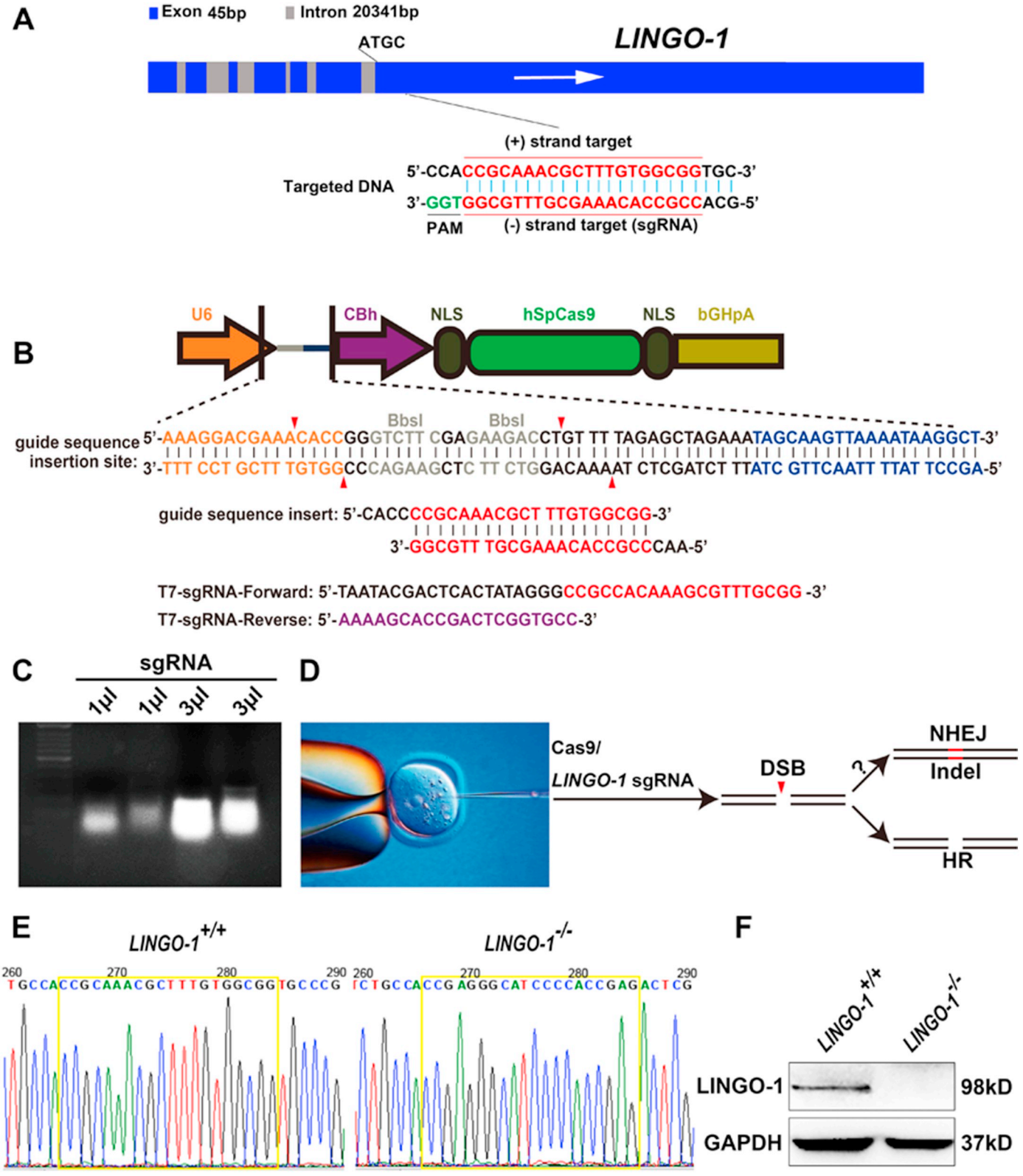

(caption on next page)

Fig. 1. Construction of *LINGO-1*$^{-/-}$ mice *using* the CRISPR/Cas9 system. (A) LINGO-1 protein coding region located at the seventh exon of the *LINGO-1* gene (the blue box with a white arrow). The designed sgRNA consisted of the DNA target sequence (red letters) directly upstream of a 5′-TGG adjacent motif (PAM, green letters). (B) Schematic diagram showing the guide sequence inserted in the pX330 plasmid (between the red arrows). The guide sequence included overhangs (black letters: 5′-CACC-3′, 5′-AAC-3′) for ligation into the BbSI sites (gray letters) in pX330. The T7 promoter was added to primers for PCR amplification using the pX330-*Cas9-LINGO-1*-sgRNA construct as the template. The PCR products were then transcribed into sgRNA containing *LINGO-1* sgRNA (red letters) and tracer RNA (dark blue letters). (C) The transcribed sgRNA was identified by agarose gel electrophoresis and the bands were present at the expected size (120 bp). (D) The Cas9 mRNA and sgRNA were microinjected into 0.5-day mouse embryos. DNA double-strand breaks (DSBs) were generated by CRISPR/Cas9 and repaired mainly through non-homologous end joining (NHEJ). If a donor with a homologous sequence flanking the DSB was utilized, DSB was mainly repaired by homologous recombination (HR). (E) Identification of homozygous gene-edited mice. DNA from F2 generation mouse tails was amplified and the amplicons were directly sequenced. Sequencing chromatograms indicated that there were no double peaks around the sgRNA target sites (sequences and peaks in yellow line boxes). Sequences starting with the fourth letter in the yellow line boxes in the *LINGO-1*$^{-/-}$ group are the edited genes. Edited genes without double peaks indicated the homozygous gene-edited mice. (F) Protein expression of homozygous gene-edited mice (*LINGO-1*$^{-/-}$) by Western blot. (For interpretation of the references to colour in this figure legend, the reader is referred to the web version of this article.)

added to the *LINGO-1* sgRNA template by PCR amplification using the following primers. The forward primer was: 5′-TAATACGACTCACTAT AGGGCCGCCACAAAGCGTTTGCGG-3′, and the reverse primer was 5′-AAAAGCACCGACTCGGTGCC-3′. The PCR product was purified using a QIAquick PCR Purification kit (QIAGEN, USA). The T7-*LINGO-1* sgRNA purified PCR product was used as the template using the MEGAshortscript T7 kit (ThermoFisher Scientific, USA) for *in vitro* transcription. Then, the transcript of *LINGO-1* sgRNA was purified using the MEGAclear kit (ThermoFisher Scientific, USA) and eluted in RNAse-free water. The quality of *LINGO-1* sgRNA was evaluated by agarose gel electrophoresis.

2.6. Microinjection into zygotes and embryo transfer

Female C57BL/6J (21–28-day-old) mice were injected with PMSG (5 IU) at 1:00–2:00 p.m. on day 1, injected with hCG (5IU) 48 h later, then housed with male C57BL/6J mice overnight. On the next morning, female mice with plugs were collected for zygote preparation (Yang et al., 2014). Zygote-cumulus complexes were collected from the oviducts, separated into single fertilized eggs in M2 medium, and then placed into KSOM medium at 37 °C in a 5% CO_2 incubator (Yang et al., 2014). *LINGO-1* sgRNA (50 ng/μl) and Cas9 mRNA (Biomics Biotechnologies, China) (100 ng/μl) diluted in injection buffer were injected into the cytoplasm of zygotes. The injected zygotes were cultured in KSOM medium at 37 °C in a 5% CO_2 incubator until the two-cell stage or the blastocyst stage, then transferred into the uteruses of surrogate female mice, and grown into F0 generation mice (Wang et al., 2013).

2.7. Identification and genotyping of transgenic mice

Mouse tails were clipped 21 days after birth, and PCR and sequencing were performed to identify and characterize founder (F0) mice. Total DNA was isolated from tails for all mice. PCR and sequencing assay were performed using the protocol described above. When mice with modified genes were identified in the F0 generation, they were selected to interbreed with WT mice. This interbreeding led to F1 generation mice, and they were identified by PCR (forward primer: 5′-TGAACCCTAAAGGAGATGGCACTG-3′, reverse primer: 5′-GTTCTCACT GATGTCCAGCTTGG-3′) and sequencing. When mice with modified genes were identified in this generation, the PCR products of genetically modified mice were analyzed by TA clone experiments. The PCR products were purified by agarose gel electrophoresis and joined with T vector. They were then transfected into DH5α competent cells. The successfully transfected cells were screened using Luria–Bertani (LB) solid medium coated with X-Gal and isopropyl β-D-thiogalactoside (IPTG). Ten white bacterial colonies were selected for sequencing analysis to characterize the modified sequence. Thereafter, male and female heterozygotes with the same modified gene sequence were mated to produce F2 generation mice, and homozygotes were screened out by PCR (primers were the same as those discussed above) and sequencing.

2.8. Spinal cord transection

Sixty-four adult female mice (56 days old) were randomly divided into two groups that underwent spinal cord transection: 1. *LINGO-1*$^{+/+}$ group (WT mice, $n = 32$); 2. *LINGO-1*$^{-/-}$ group (*LINGO-1* KO homozygote mice, $n = 32$). All animals were anesthetized with 1% sodium pentobarbital (6.67 μl/g, i.p.). A dorsal laminectomy was performed at the T9 vertebral level to expose the T9 and T10 spinal cord segments. The dura mater, arachnoid, and pia mater were slit open successively, and then the T10 segment of the spinal cord was transected completely with a straight trabecular scissors. The transection site was carefully examined and the wound was sutured after thorough hemostasis. Dysfunction of bladder control was a transient side effect in all mice that underwent spinal cord transection. Manual emptying of the bladders was performed 3 times per day. After surgery, the mice received an intramuscular injection of penicillin (32,000 U/ml/day) within the first 3 days to prevent infection. Both groups of mice were sacrificed 14 days after transection.

2.9. Morphological analysis

Fourteen days after spinal cord transection, some of the injured mice ($n = 8$ for each group) and normal mice ($n = 3$ for each group) were anesthetized with 2% sodium pentobarbital (13.34 μl/g, i.p.), then transcardially perfused with 0.1 M phosphate buffer (PB) pH 7.4, followed by 4% paraformaldehyde, then post-fixed with 4% paraformaldehyde for 24 h, and dehydrated with 30% phosphate-buffered sucrose (PBS) at 4 °C for 72 h. Normal spinal cord tissue at C4–C5, T9–T10, and L3–L5, and injured spinal cord at T8–T12 were embedded in Tissue Tek O.C.T compound (Sakura Finetek, Torrance, CA, USA). Coronal sections of normal spinal cord segments and longitudinal sections of injured spinal cord at T8–T12 were cut into 20-μm–thick slices using a cryostat microtome. The coronal sections were processed for neutral red staining. The longitudinal sections were processed for immunohistochemistry (IHC) staining as previously described (Guo et al., 2007). *In situ* cell death around the SCI site was detected according to the manufacturer's protocol (*In Situ* Cell Death Detection Kit, TMR red, 12,156,792,910, Roche). The primary antibodies used for immunofluorescence were as follows: APC (1:100, Abcam, ab15270, USA), MAP2 (1:2500, Abcam, ab92434, USA), LINGO-1 (1:500, Abcam, ab23631, USA), IBA1 (1:300, Wako, CTK6675, USA), GFAP (1:500, Abcam, ab7260, USA), CSPGs (1:500, Sigma, SAB4200696, USA), NF (1:200, Biolegend, 837,904, USA), CGRP (1:100, Abcam, ab81887, USA), and 5-HT (1:8000, Sigma, S5545, USA). Species-specific secondary antibodies (1:1000, ThermoFisher Scientific, Alexa Fluor 488 goat anti-mouse IgG, A11001; 1:1000, ThermoFisher Scientific, Alexa Fluor 488 goat anti-rabbit IgG, A11008; 1:1000, ThermoFisher Scientific, Alexa Fluor 488 goat anti-chicken IgG, A11039; 1:1000, ThermoFisher Scientific, Alexa Fluor 555 goat anti-rabbit IgG, A27039) were used for detection of specific antigenic sites. Hoechst33342 (1:1000, ThermoFisher Scientific, H1399, USA) was used for nuclear staining. The slides were visualized and images captured using a

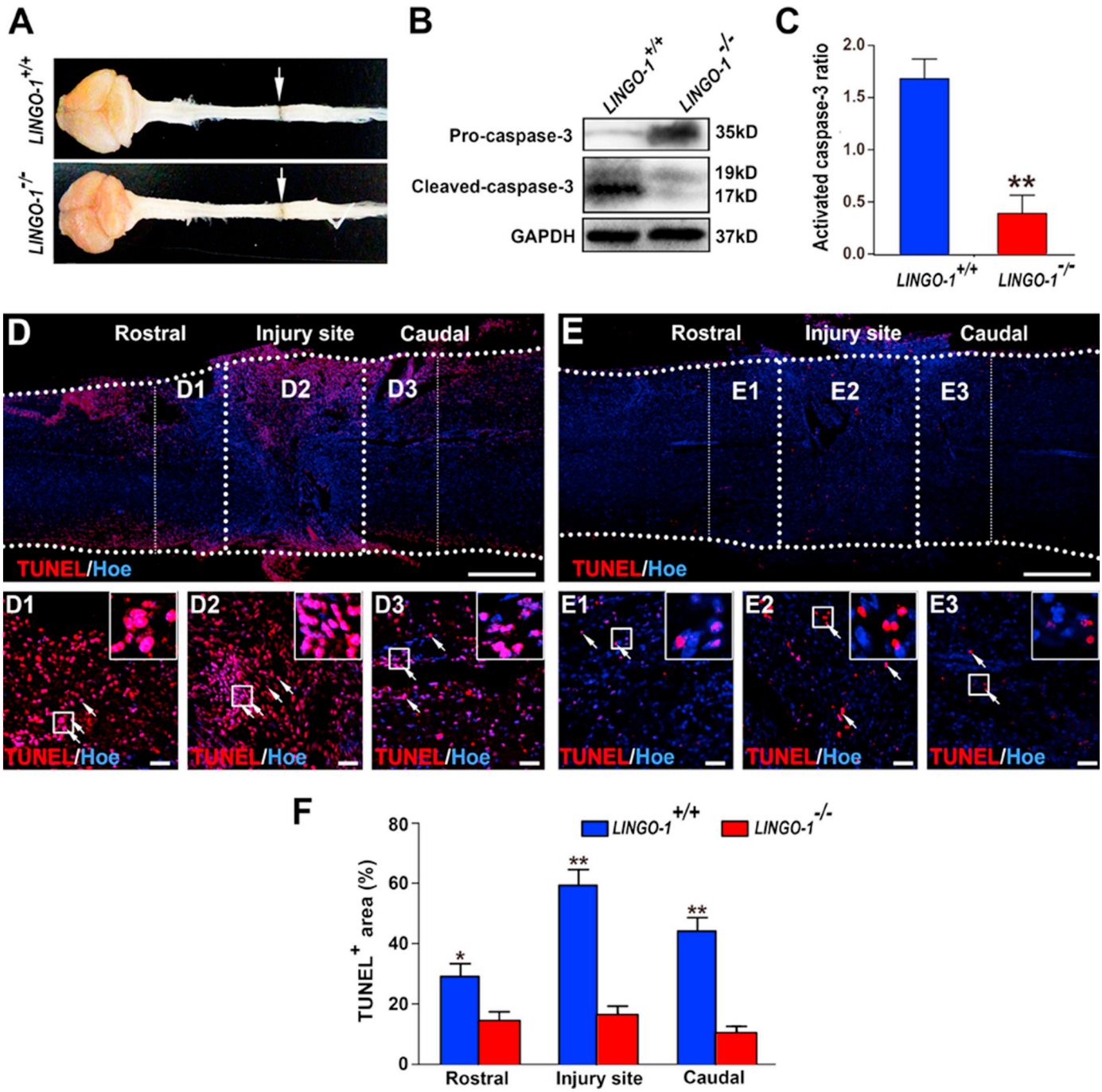

Fig. 2. Apoptosis in injured tissues after spinal cord injury (SCI). (A) Arrows showing the SCI sites at 14 days after injury. (B) Expression of pro-caspase-3 and cleaved-caspase-3 in the SCI site. GAPDH protein expression was used as a loading control. (C) Bar chart showing the protein expression ratio of cleaved-caspase-3/pro-caspase-3 in the SCI site in the *LINGO-1*$^{+/+}$ and *LINGO-1*$^{-/-}$ groups. $^{**}P < 0.01$. (D) Transferase-mediated deoxyuridine triphosphate biotin nick end labeling (TUNEL)-positive cells were widely distributed in longitudinal sections of transected spinal cords in the *LINGO-1*$^{+/+}$ group. Enlarged view of TUNEL-positive cells (red, white arrows) in the rostral area (D1), injury site (D2), and caudal area (D3) of spinal cords in the *LINGO-1*$^{+/+}$ group. (E) TUNEL-positive cells in a longitudinal section of a transected spinal cord in the *LINGO-1*$^{-/-}$ group. High magnification of TUNEL-positive cells (red, white arrows) in the rostral area (E1), injury site (E2), and caudal area (E3) of a spinal cord in the *LINGO-1*$^{-/-}$ group. (F) Bar chart showing the percentage of TUNEL-positive areas in the *LINGO-1*$^{+/+}$ and *LINGO-1*$^{-/-}$ groups. $^{*}P < 0.05$, $^{**}P < 0.01$. All cell nuclei of TUNEL-positive cells were counterstained with Hoechst33342 (Hoe). Scale bars = 500 μm in (D)–(E) and 20 μm in (D1)–(E3). (For interpretation of the references to colour in this figure legend, the reader is referred to the web version of this article.)

confocal fluorescence microscope (Zeiss, Germany).

2.10. Western blot analysis in mice

At 3, 7, and 14 days after spinal cord transection, some of the mice ($n = 8$ for each group) were deeply anesthetized and sacrificed using 2% sodium pentobarbital (13.34 μl/g, i.p.). A 1-cm segment of the spinal cord extending from T8 to T11 containing the injury site was quickly dissected on ice. Protein from the spinal cord segments was extracted using protein lysis buffer (Huang et al., 2014) and quantified using a BCA protein assay kit (Thermo Scientific, USA). Equal amounts of the protein suspension were separated by 12% sodium

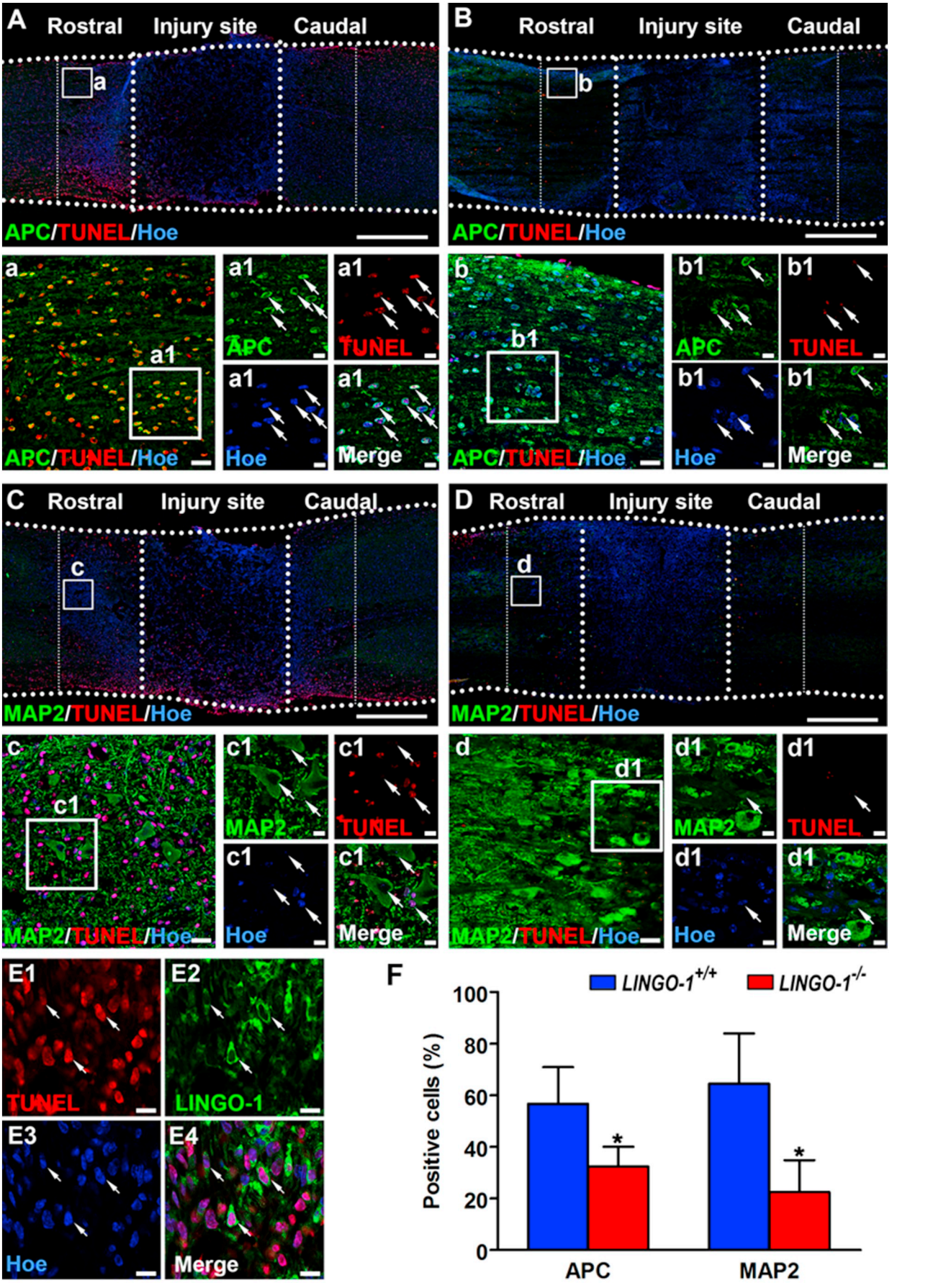

(caption on next page)

Fig. 3. Transferase-mediated deoxyuridine triphosphate biotin nick end labeling (TUNEL) co-labeling with APC-, MAP2-, and LINGO-1-positive cells in the injured spinal cord. (A) and (B) TUNEL/APC immunofluorescence staining in longitudinal sections of injured spinal cord white matter in the *LINGO-1*$^{+/+}$ (A) and *LINGO-1*$^{-/-}$ (B) groups. Magnified TUNEL-positive cells (red, white arrows) and APC-positive cells (green, white arrows) in the *LINGO-1*$^{+/+}$ group (a, a1) and in the *LINGO-1*$^{-/-}$ group (b, b1). (C) and (D) TUNEL-/MAP2-positive cells in longitudinal sections of transected spinal cord gray matter in the *LINGO-1*$^{+/+}$ (C) and *LINGO-1*$^{-/-}$ (D) groups. Magnified TUNEL-positive cells (red, white arrows) and MAP2-positive cells (green, white arrows) in the *LINGO-1*$^{+/+}$ group (c, c1) and the *LINGO-1*$^{-/-}$ group (d, d1). (E1)–(E4) TUNEL-/LINGO-1-/Hoechst33342-positive labeled cells (white arrows) and merged images in the *LINGO-1*$^{+/+}$ group. (F) The percentage of TUNEL-/APC-positive cells in TUNEL-positive cells, and the percentage of TUNEL/MAP2-positive cells in TUNEL- positive cells around the injury sites in the *LINGO-1*$^{+/+}$ and *LINGO-1*$^{-/-}$ groups. Asterisks indicated statistically significance differences (*$P < 0.05$) between the *LINGO-1*$^{+/+}$ and *LINGO-1*$^{-/-}$ groups. All cell nuclei were counterstained with Hoechst33342 (Hoe). Scale bars = 500 μm in (A)–(D), 50 μm in (a)–(d), and 10 μm in (a1)–(d1) and (E1)–(E4). (For interpretation of the references to colour in this figure legend, the reader is referred to the web version of this article.)

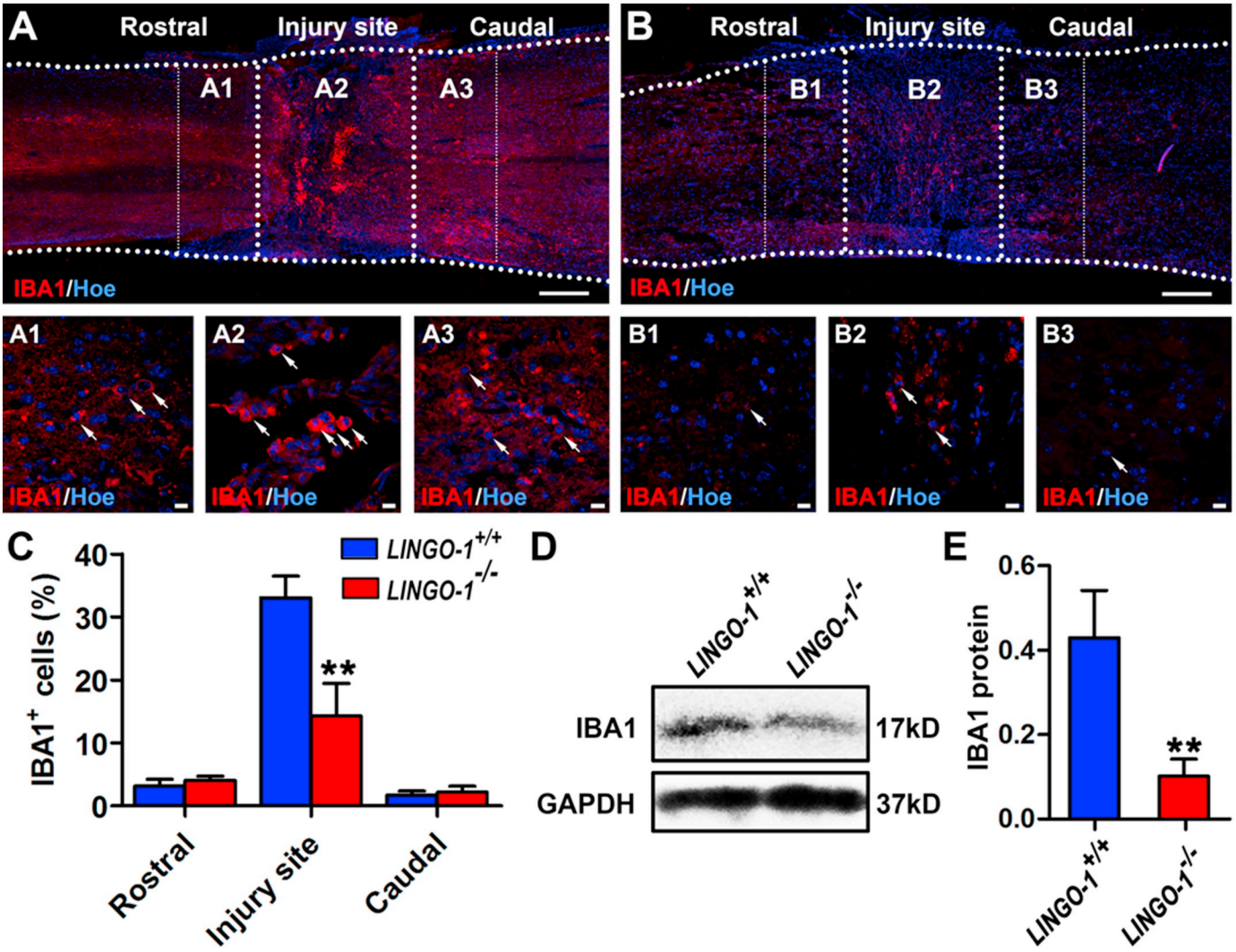

Fig. 4. IBA1-positive cells in the injured spinal cord. (A) IBA1-positive cells in a longitudinal section of transected spinal cord in the *LINGO-1*$^{+/+}$ group. Enlarged view of IBA1-positive cells (red, white arrows) in the rostral area (A1), injury site (A2), and caudal area (A3) of the spinal cord. (B) IBA1-positive cells in a longitudinal section of transected spinal cord in the *LINGO-1*$^{-/-}$ group. Magnified IBA1-positive cells (red, white arrows) in the rostral area (B1), injury site (B2), and caudal area (B3) of the spinal cord. (C) Percentage of IBA1-positive cells in the injury site and the areas rostral and caudal to the injury site in the *LINGO-1*$^{+/+}$ and *LINGO-1*$^{-/-}$ groups. (D) Expression of IBA1 in the spinal cord injury (SCI) site, with GAPDH protein bands used as loading controls. (E) Bar chart showing IBA1 levels in the SCI site in the *LINGO-1*$^{+/+}$ and *LINGO-1*$^{-/-}$ groups. Asterisks indicate statistically significant differences (**$P < 0.01$). All cell nuclei of IBA1-positive cells were counterstained with Hoechst33342 (Hoe). Scale bars = 500 μm in (A)–(B) and 20 μm in (A1)–(B3). (For interpretation of the references to colour in this figure legend, the reader is referred to the web version of this article.)

dodecylsulfate-polyacrylamide gel electrophoresis (SDS-PAGE) and transferred to polyvinylidene fluoride (PVDF) membranes. The membranes were incubated with rabbit anti-LINGO-1 antibody (1:1000, Abcam, ab23631, USA), rabbit anti-caspase-3 antibody (1:1000, CST, 9662S, USA), rabbit anti-cleaved-caspase-3 antibody (1:1000, CST, 9664S, USA), rabbit anti-IBA1 antibody (1:1000, Wako, CTK6675, USA), mouse anti-GFAP antibody (1:1000, Abcam, ab7260, USA), mouse-anti-CSPGs antibody (1:1000, Sigma, SAB4200696, USA), rabbit anti-NF200 antibody (1:1000, Sigma, N4142, USA), and mouse anti-GAPDH antibody (1:10,000, Sigma, G8795, USA) at 4 °C overnight, followed by incubation with secondary anti-rabbit HRP-conjugated IgG (1:2500, CST, 7077S, USA) and anti-mouse HRP-conjugated IgG (1:2500, CST, 7076S, USA). The bands were visualized using an enhanced chemiluminescence (ECL) Western blot detection kit (Millipore,

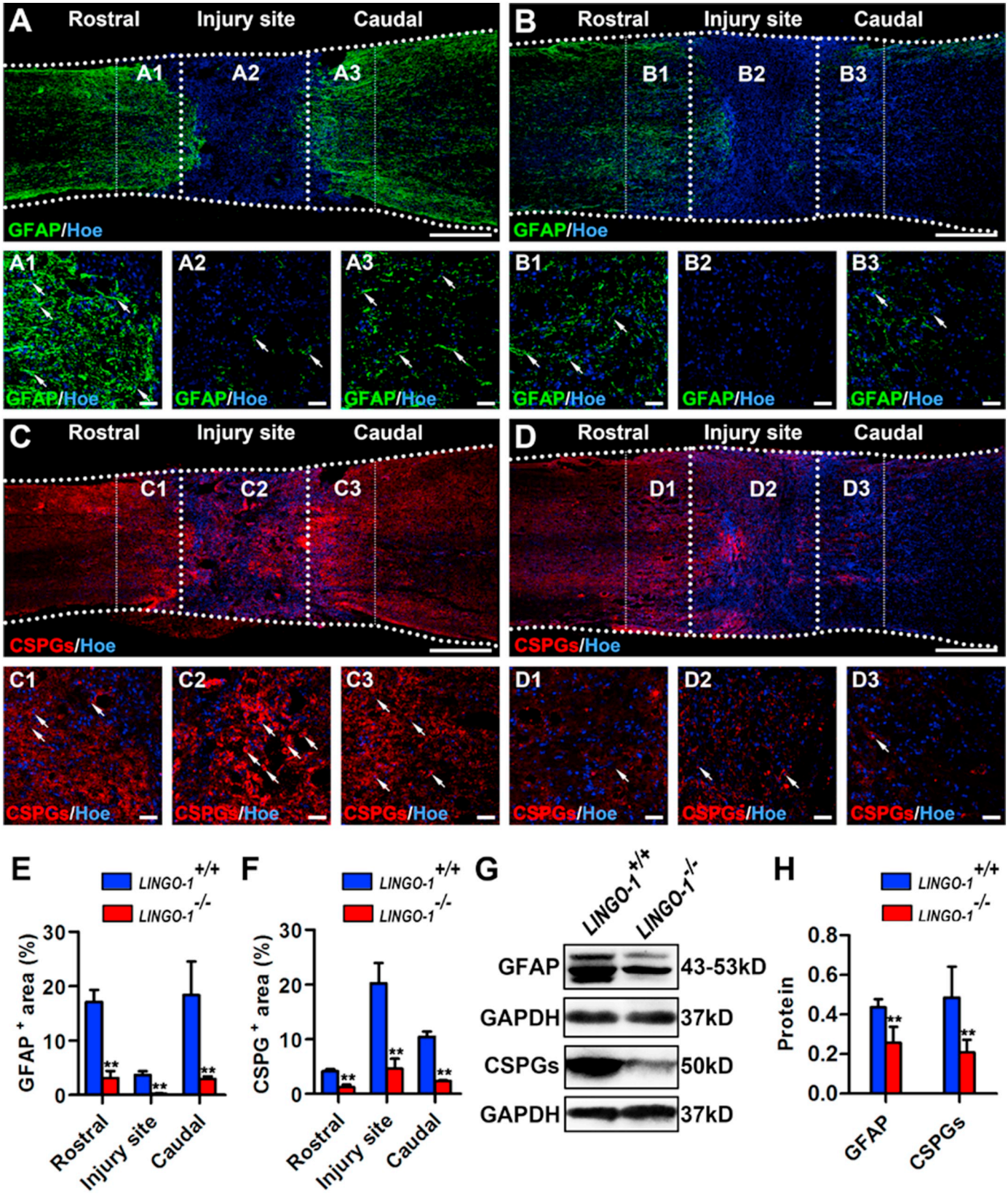

(caption on next page)

Fig. 5. Glial fibrillary acidic protein (GFAP)- and CSPG-positive areas in the injured spinal cord. (A) and (B) GFAP immunofluorescence staining of longitudinal sections of injured spinal cord in the *LINGO-1*$^{+/+}$ (A) and *LINGO-1*$^{-/-}$ (B) groups. Magnified GFAP-positive areas (green, white arrows) in the areas rostral (A1) and caudal (A3) to the injury site (A2) of spinal cord in the *LINGO-1*$^{+/+}$ group, and in the areas rostral (B1) and caudal (B3) to the injury site (B2) of spinal cord in the *LINGO-1*$^{-/-}$ group. (C) and (D) CSPG-positive areas in longitudinal sections of transected spinal cord in the *LINGO-1*$^{+/+}$ (C) and *LINGO-1*$^{-/-}$ (D) groups. Magnified CSPG-positive areas (red, white arrows) in the *LINGO-1*$^{+/+}$ group (C1)–(C3) and the *LINGO-1*$^{-/-}$ group (D1)–(D3). (E) and (F) Percentages of GFAP-positive (E) and CSPG-positive (F) areas in the injury site and the areas rostral and caudal to the spinal cord injury (SCI) site in the *LINGO-1*$^{+/+}$ and *LINGO-1*$^{-/-}$ groups. (G) Expression of GFAP and CSPGs in the SCI site with GAPDH protein bands used as loading controls. (H) Bar chart showing GFAP and CSPG levels in the SCI site in the *LINGO-1*$^{+/+}$ and *LINGO-1*$^{-/-}$ groups. Asterisks indicate statistically significant differences (**$P < 0.01$) between the *LINGO-1*$^{+/+}$ and *LINGO-1*$^{-/-}$ groups. All cell nuclei were counterstained with Hoechst33342 (Hoe). Scale bars = 500 μm in (A)–(D) and 20 μm in (A1)–(D3). (For interpretation of the references to colour in this figure legend, the reader is referred to the web version of this article.)

WBKLS0500, USA). The gray value of bands was analyzed using Image J.

2.11. Morphological quantification

To observe the areas 0.5 mm rostral and 0.5 mm caudal to the injury site, as well as the SCI site, every fifth longitudinal section from each spinal cord was evaluated. Twenty-five sections taken from each mouse were immunostained with transferase-mediated deoxyuridine triphosphate biotin nick end labeling (TUNEL), APC, MAP2, IBA1, GFAP, CSPGs, and NF antibodies. The stained sections were imaged and analyzed using a TissueFAXS 200 flow-type tissue quantitative analyzer (TissueGnostics GmbH, Vienna, Austria). Expression of the proteins listed above was performed in the injured region, and the areas 0.5 mm rostral and 0.5 mm caudal to the injury site, as demarcated by 4 red lines (Fig. S1). The percentage of apoptotic oligodendrocytes and neurons was obtained by counting APC/TUNEL- and MAP2/TUNEL-positive cells with well-delineated nuclei counterstained with Hoechst33342. The percentage of microglial cells/macrophages was obtained by counting IBA1-positive cells with well-delineated nuclei counterstained with Hoechst33342. We used GFAP and CSPG immunofluorescence staining to identify glial scars, and NF immunoreactive staining to determine the number of NF-positive nerve fibers. The area percentages occupied by the glial scars and nerve fibers were determined from the ratio of the positive immunoreactive area to the total tissue area between the two red lines (Fig. S1).

2.12. Statistical analysis

The data were analyzed using Student's *t*-test and presented as means ± standard deviation (SD). Statistical significance was calculated using the statistical software SPSS 13.0. $P < 0.05$ was considered statistically significant.

3. Results

3.1. Generation of LINGO-1$^{-/-}$ mice

To assess the effect of LINGO-1 on SCI, we designed an sgRNA which was cloned into a pX330 plasmid expressing Cas9 and driven by the U6 promoter (Fig. 1A, B, Fig. S2A). PCR products from NSCs transfected with pX330-Cas9-*LINGO-1* vector exhibited double peaks in the region corresponding to sgRNA (Fig. S2B, C). The sgRNA band indicated that the sgRNA was successfully obtained (Fig. 1C). The *LINGO-1* sgRNA and Cas9 mRNA were co-injected into one-cell embryos (Fig. 1D), and 1 female mouse and 6 male mice were generated for the F0 generation (Table S1, Fig. S3A). TA cloning analysis of genetically modified mice in the F1 generation showed that there were five different mutations in the *LINGO-1* gene (Fig. S3B), and homozygous mice with the 23 bp deletion in the F2 generation were obtained (Table S2, Fig. 1E). The central nervous tissue of homozygous mice with the 23 bp deletion was evaluated for LINGO-1 expression by Western blot, and the results showed that there was no band in the *23 bp-LINGO-1*$^{-/-}$ mice compared with the *LINGO-1*$^{+/+}$ mice (Fig. 1F), suggesting that the *LINGO-1*$^{-/-}$ mice had been constructed successfully using the CRISPR/Cas9 system. To determine whether there were spinal cord abnormalities in adult *LINGO-1*$^{-/-}$ mice, the proportion of gray matter to white matter at C4–C5, T9–10, and L3–L5 was determined by neutral red staining, which showed no obvious differences between *LINGO-1*$^{+/+}$ and *LINGO-1*$^{-/-}$ mice (Fig. S4).

3.2. Cell apoptosis in the SCI site of LINGO-1 KO mice

We examined the effect of LINGO-1 on cell apoptosis by implementing a T9 and T10 transection SCI model. The spinal cord, including the lesion site, was removed at 14 days after SCI (Fig. 2A). LINGO-1 expression was up-regulated significantly at 14 days after SCI in *LINGO-1*$^{+/+}$ mice, and there was no LINGO-1 expression at any time point in *LINGO-1*$^{-/-}$ mice (Fig. S5A, B). Widespread apoptosis, as evidenced by increased expression of cleaved-caspase 3 protein in the cord tissue, was obvious, and was significantly improved at 14 days compared with 3 days after SCI (Fig. S5A, C). However, when *LINGO-1* was deleted, the expression of cleaved caspase-3, which can induce apoptosis, was significantly down-regulated in the injured tissue of *LINGO-1*$^{-/-}$ mice compared with *LINGO-1*$^{+/+}$ mice at each time point (Fig. 2B,C, Fig. S5A, C). TUNEL immunoreactivity was quantified at the following three regions of the spinal cord: rostral area, injury site, and caudal area. The percentage of TUNEL-positive cells in each area was calculated (Fig. S1). The results showed that the TUNEL-positive areas were significantly smaller in the *LINGO-1*$^{-/-}$ group compared with those in the *LINGO-1*$^{+/+}$ group (Fig. 2D–F). This indicated that deletion of *LINGO-1* can protect cells from apoptosis after SCI.

3.3. Rescue of oligodendrocytes and neurons in LINGO-1 KO mice

To determine whether apoptotic cells were associated with LINGO-1 expression, we co-labeled apoptotic cells around the injury site with LINGO-1 in *LINGO-1*$^{+/+}$ mice, which showed co-localization of LINGO-1 and TUNEL (Fig. 3E1–E4). Previous reports showed that LINGO-1 was present in oligodendrocytes and neurons (Mi et al., 2004; Mi et al., 2005). To determine the types of apoptotic cells, oligodendrocytes (APC) and neurons (MAP2) were each co-labeled with TUNEL. The results showed that the apoptotic cells were co-localized with APC (Fig. 3A–B) and MAP2 (Fig. 3C–D). The sum of cells positive for APC/TUNEL and MAP2/TUNEL was determined for the rostral area, injury site, and caudal area (Fig. S1). Compared with the *LINGO-1*$^{+/+}$ group, apoptosis in oligodendrocytes and neurons was significantly reduced in the *LINGO-1*$^{-/-}$ group (Fig. 3F). These results suggested that LINGO-1-positive cells underwent apoptosis in WT mice and that apoptosis occurred in oligodendrocytes and neurons, which was rescued by *LINGO-1* KO.

3.4. Inflammation in the SCI site in LINGO-1 KO mice

To observe the inflammatory response following spinal cord transection, we evaluated IBA1 expression in WT and *LINGO-1* KO mice at 14 days after SCI by immunofluorescence staining (Fig. 4A–B). IBA1 is a macrophage/microglia-specific calcium-binding protein that plays a key role in membrane ruffling and phagocytosis (Ohsawa et al., 2000). We found that IBA1-positive cells accumulated mainly at the SCI site

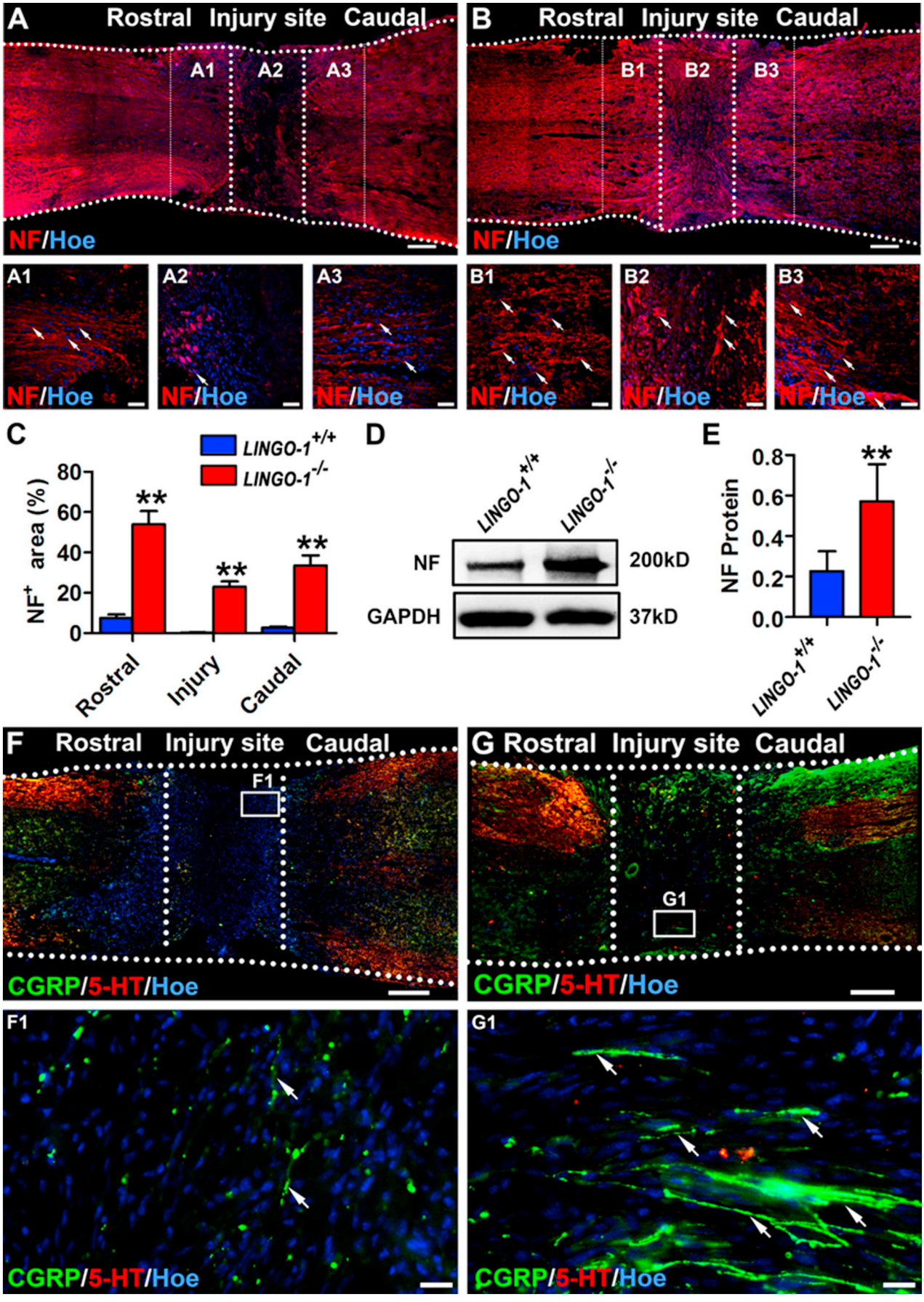

(caption on next page)

Fig. 6. Neurofilament (NF)-positive areas in the injured spinal cord. (A) and (B) NF immunofluorescence staining showing longitudinal sections of injured spinal cord in the *LINGO-1*$^{+/+}$ group (A) and the *LINGO-1*$^{-/-}$ group (B). Magnified NF-positive areas (red, white arrows) in the areas rostral (A1) and caudal (A3) to the injury site (A2) in the *LINGO-1*$^{+/+}$ group, and in the areas rostral (B1) and caudal (B3) to the injury site (B2) in the *LINGO-1*$^{-/-}$ group. (C) Bar chart showing the percentage of NF-positive areas in the injury site and areas rostral and caudal to the SCI site in the *LINGO-1*$^{+/+}$ and *LINGO-1*$^{-/-}$ groups. (D) Expression of NF in the SCI site with GAPDH protein bands used as loading control. (E) Bar chart showing the NF level in the SCI site in the *LINGO-1*$^{+/+}$ and *LINGO-1*$^{-/-}$ groups. (F) and (G) CGRP and 5-HT immunofluorescence co-staining of longitudinal sections of injured spinal cord in the *LINGO-1*$^{+/+}$ group (F) and the *LINGO-1*$^{-/-}$ group (G). Magnified CGRP-positive areas (green, white arrows) and 5-HT–positive areas (red) in the SCI site (F1) in the *LINGO-1*$^{+/+}$ group, and in the injury site (G1) in the *LINGO-1*$^{-/-}$ group. Asterisks indicate statistically significant differences (**$P < 0.01$) between the *LINGO-1*$^{+/+}$ and *LINGO-1*$^{-/-}$ groups. All cell nuclei were counterstained with Hoechst33342 (Hoe). Scale bars = 500 μm in (A)–(B), 20 μm in (A1)–(B3), and 50 μm in (F1)–(G1). (For interpretation of the references to colour in this figure legend, the reader is referred to the web version of this article.)

(Fig. 4A2, B2). In addition, IBA1-positive cells were also detected in the rostral and caudal areas near the injury site (Fig. 4A1, A3, B1, B3) in the *LINGO-1*$^{+/+}$ and *LINGO-1*$^{-/-}$ groups. IBA1 immunoreactivity was quantified in three regions: the rostral area, injury site, and caudal area (Fig. S1). There were no statistically significant differences in the number of IBA1-positive cells in the rostral and caudal areas of spinal cord between the *LINGO-1*$^{+/+}$ and *LINGO-1*$^{-/-}$ groups. However, in the injury site, the number of IBA1-positive cells was significantly lower in the *LINGO-1*$^{-/-}$ group (14.25 ± 5.17) compared with the *LINGO-1*$^{+/+}$ group (33.05 ± 3.46; Fig. 4A–C). Western blot was performed to quantify the level of inflammation in the injured spinal cord further. IBA1 expression was lower in the *LINGO-1*$^{-/-}$ group (0.10 ± 0.04) than in the *LINGO-1*$^{+/+}$ group (0.43 ± 0.11; Fig. 4D, E). These results suggested that deletion of *LINGO-1* can reduce the number of microglial cells/macrophages in the SCI site, resulting in reduction of inflammation after SCI.

3.5. Glial scar formation in the SCI site in LINGO-1 KO mice

GFAP is a marker of reactive astrocytes and CSPGs are secreted by astrocytes. Increased expression levels of GFAP and CSPGs may reflect glial scar formation (Jo et al., 2018). We examined the expression of GFAP and CSPGs in spinal cord tissue 14 days after SCI using immunofluorescence staining. After SCI, GFAP-positive cells were markedly increased at the broken areas of the injury site, seemingly forming an astrocytic wall (Fig. 5A, A1, A3) in the *LINGO-1*$^{+/+}$ group. Very few GFAP-positive cells were present in the injury site (Fig. 5A2). Many GFAP-positive cells were present at the border of the injury site in the *LINGO-1*$^{-/-}$ group, but the immunoreactivity was noticeably less intense (Fig. 5B, B1–B3) when compared with that in the *LINGO-1*$^{+/+}$ group. Although CSPG immunofluorescence was ubiquitous in the injury site of spinal cord (Fig. 5C-D) , CSPG immunofluorescence was markedly reduced in the *LINGO-1*$^{-/-}$ group (Fig. 5D, D1-D3) when compared with that in the *LINGO-1*$^{+/+}$ group (Fig. 5C, C1-C3). Statistical analysis showed that GFAP and CSPG immunoreactivity was significantly decreased in the *LINGO-1*$^{-/-}$ group compared with that in the *LINGO-1*$^{+/+}$ group (Fig. 5E–F). The percentage of GFAP immunoreactive area in the rostral, caudal, and injury sites was 17.09 ± 2.19, 18.34 ± 6.15, and 3.66 ± 0.70, respectively, in the *LINGO-1*$^{+/+}$ group (Fig. 5E). However, the *LINGO-1*$^{-/-}$ group (Fig. 5E) had a smaller percentage of GFAP immunoreactivity area in the rostral (3.13 ± 1.27), caudal (2.94 ± 0.74), and injury sites (0.21 ± 0.11). In the *LINGO-1*$^{+/+}$ group (Fig. 5F), the percentage of CSPG immunoreactive area in the rostral, caudal, and injury sites was 4.15 ± 0.42, 10.45 ± 0.94 and 20.23 ± 3.71, respectively. In contrast, in the *LINGO-1*$^{-/-}$ group (Fig. 5F), the percentage of CSPG immunoreactive area in the rostral (1.27 ± 0.41), caudal (2.35 ± 0.14), and injury sites (4.60 ± 1.83) was significantly lower than in the corresponding areas in WT mice. Western blot also showed that GFAP and CSPGs were significantly down-regulated in the *LINGO-1*$^{-/-}$group (0.26 ± 0.08, 0.21 ± 0.06) compared with the *LINGO-1*$^{+/+}$ group (0.44 ± 0.04, 0.49 ± 0.16) (Fig. 5G–H). The results demonstrated that *LINGO-1* deletion can reduce the formation of glial scar after SCI.

3.6. Nerve fiber regeneration in the SCI site in LINGO-1 KO mice

At 14 days after SCI, immunofluorescence staining was performed to detect the expression level of NF, a nerve fiber marker, in the areas rostral and caudal to the injury site of the transected spinal cord. The results showed an increased amount of NF in the *LINGO-1*$^{-/-}$ group compared to that in the *LINGO-1*$^{+/+}$ group (Fig. 6A–B). At higher magnification, immunofluorescence was noticeably more intense in the areas rostral and caudal to the SCI site in the *LINGO-1*$^{-/-}$ group than that in the *LINGO-1*$^{+/+}$ group. Of note, the increase in NF-positive area in the injury site was more pronounced in the *LINGO-1*$^{-/-}$ group (Fig. 6B2). NF-positive nerve fibers were parallel in the *LINGO-1*$^{+/+}$ group (Fig. 6A1, A3), while those in the *LINGO-1*$^{-/-}$ group tended to be twisted in the rostral and caudal areas (Fig. 6B1, B3). In addition, quantitative evaluation (Fig. 6C) showed that the percentage of NF-positive areas in the rostral (54.02 ± 6.50), caudal (33.62 ± 5.02), and injury sites (23.12 ± 2.63) was significantly increased in the *LINGO-1*$^{-/-}$ group when compared with the corresponding area in rostral (7.62 ± 1.74), caudal (2.80 ± 0.54), and injury sites (0.34 ± 0.21) in the *LINGO-1*$^{+/+}$ group. The results were consistent with Western blot results (Fig. 6D, E), which showed that NF expression at the SCI site in the *LINGO-1*$^{-/-}$ group (0.54 ± 0.18) was significantly increased compared to that in the *LINGO-1*$^{+/+}$ group (0.20 ± 0.73). Many CGRP-positive ascending nerve fibers were also observed in the SCI site in *LINGO-1*$^{-/-}$ mice, but 5-HT–positive descending nerve fibers appeared in large quantities at the boundary between rostral and injury site and only a small amount in the lesion site (Fig. 6G). In the injury site and boundary site of *LINGO-1*$^{+/+}$ mice, both CGRP- and 5-HT–positive nerve fibers were sparse (Fig. 6F). These data suggested that deletion of *LINGO-1* promotes the regeneration of nerve fibers in the injured spinal cord, expecially CGRP positive nerve fibers.

4. Discussion

In the present study we investigated post-SCI cell survival, inflammation, glial scar formation, and nerve fiber regeneration in mice lacking LINGO-1. We demonstrated that *LINGO-1* KO may decrease cell apoptosis, attenuate inflammation, and reduce glial scar formation. Furthermore, we provide evidence that *LINGO-1* KO can enhance nerve fiber regeneration in the injury site after SCI.

In traditional genetically modified mice, modified exogenous DNA is inserted through homologous recombination in mouse embryonic stem cells (ESCs) using conventional gene-targeting methods, and the targeted ESCs are injected into WT blastocysts to generate chimeric mice containing the targeted gene modification (Capecchi, 2005). This method is costly and time-consuming (Wang et al., 2013). Co-injection of Cas9 mRNA and sgRNAs into zygotes also generates mice with biallelic mutations of targeted genes with high efficiency (Wang et al., 2013). Compared with previous gene-editing techniques, the CRISPR/Cas9 system allows for rapid, efficient, and cost-effective genetic modification. Hence, this system has been widely used as a powerful genome-editing tool for producing genetically modified cell lines and animal models (Chen et al., 2015; Platt et al., 2014; Wang et al., 2013). The CRISPR/Cas9 technology was suitable for generation of

homozygous *LINGO-1* KO mice.

Previous studies showed that SCI induced cell death, inflammation, and glial scar formation, which inhibited nerve fiber growth and formation of synapses (Silver and Miller, 2004; Tran et al., 2018). SCI disrupts motor, sensory, and autonomic functions, which can cause limb paralysis (Lai et al., 2013; Lu et al., 2018; Ren et al., 2018). Michael et al. reported that cell apoptosis was observed 6 h after SCI, and lasted for many weeks, particularly oligodendrocyte apoptosis, which resulted in demyelination of white matter tracts (Beattie et al., 2000; Mizuno et al., 1998). Apoptosis occurs in two stages: the initial phase involves apoptosis of multiple cell types at the lesion center, and the later phase involves apoptosis of oligodendrocytes and microglial cells (Beattie et al., 2000). Apoptotic cells included neurons, oligodendrocytes, and microglial cells, but not astrocytes (Beattie et al., 2000; Crowe et al., 1997; Li et al., 1996; Shuman et al., 1997). LINGO-1 is a negative regulator of neuron and oligodendrocyte survival, nerve fiber regeneration, myelination, and functional recovery (Andrews and Fernandez-Enright, 2015). To investigate the protective role of *LINGO-1* KO on SCI, *LINGO-1*$^{-/-}$ mice underwent spinal cord transection. In the present study, LINGO-1 expression significantly increased from 3 to 14 days after SCI in WT mice, which corresponded with increased expression of activated caspase-3. Interestingly, we found that *LINGO-1* KO significantly reduced the incidence of apoptosis in the injured spinal cord compared to that in WT mice. In *LINGO-1*$^{+/+}$ mice, apoptotic cells, including oligodendrocytes and neurons, expressed LINGO-1, and this apoptosis was rescued by deletion of *LINGO-1*. These results suggested that LINGO-1 contributed to cell apoptosis and that *LINGO-1* KO may be a promising strategy to promote cell survival after SCI. These results were consistent with results presented by Ji et al. using a LINGO-1 antagonist (Ji et al., 2006). *LINGO-1* KO may protect cells from apoptosis, by activating the EGFR/PI3-K/Akt pathway (Inoue et al., 2007), promotion of WNK3 kinase activity (Zhang et al., 2013), up-regulation of phospho-TrkB phosphorylation, and activation of the BDNF/TrkB signaling pathway (Fu et al., 2010; Fu et al., 2009) and decreasing caspase-3 expression and inhibition of RhoA/Rho-kinase (RhoA/Rock) pathway (Ji et al., 2006). In the present study, we demonstrated that LINGO-1 plays a direct role in cell apoptosis in injured spinal cord, but identification of surviving cells and signaling pathways involved in protection against apoptosis has not been performed. Increased cell survival may promote nerve fiber regeneration in *LINGO-1* KO mice.

As documented previously by our group and others, SCI elicits acute inflammation, which is typically caused by physical injury and factors released from dead cells (Bianchi, 2007). In an acute inflammatory environment in the central nervous system, microglial cells migrate to the lesion area (Davalos et al., 2005; Gadani et al., 2015; Wu et al., 2005), resulting in a shift from M2-polarization to M1-polarization (Gwak and Hulsebosch, 2009; Kigerl et al., 2009). This polarization exacerbates inflammation, causing further loss of neurons and increased astrogliosis in the SCI site (Wang et al., 2015). IBA1 is a microglia−/macrophage-specific calcium-binding protein involved in cell membrane ruffling and phagocytosis (Ito et al., 1998; Ohsawa et al., 2000). Although inflammatory cells may contribute to clearing of cellular debris from the injury site and help to prevent the spread of the lesion (Hines et al., 2009), they also contribute to demyelination and are involved in nerve fiber injury (Weiner, 2008). Furthermore, cytokines released during the inflammatory response can damage oligodendrocytes and nerve fibers (Ruggieri et al., 2017). Therefore, novel strategies to decrease inflammation and promote effective recovery after SCI are of great interest. LINGO-1, a negative regulator, suppresses axonal regeneration, oligodendrocyte precursor cell maturation, and myelination in neurological disorders (Andrews and Fernandez-Enright, 2015; Foale et al., 2017). Our data showed that IBA1 expression in the SCI site after SCI in *LINGO-1*$^{-/-}$ mice was markedly attenuated when compared to that in WT mice, indicating that absence of LINGO-1 in mice may negatively regulate the spread of inflammation in SCI. Although downstream pathways of LINGO-1 were not examined in this study, a previous study by Paschalis Theotokis and colleagues showed that NgR, LINGO-1, and TROY complex were expressed in macrophages in the acute phase, and negatively regulated GAP-43^{+} axonal growth (Theotokis et al., 2016). These results agreed with our findings that *LINGO-1*$^{-/-}$ contributed to inflammatory regulation by creating an anti-inflammatory microenvironment, which promoted nerve fiber regeneration.

Inflammatory cells infiltrating the SCI site activate resident glial cells, such as astrocytes and oligodendrocytes progenitor cells (Tran et al., 2018). Reactive astrocytes surrounding the lesion site create a wall-like structure with thick hypertrophied processes of overlapping outgrowths (Wanner et al., 2013), which forms the glial scar boundary (Orr and Gensel, 2018). The border formed by astrocytes also produces potently inhibitory molecules, such as CSPGs (Anderson et al., 2016; Orr and Gensel, 2018; Schachtrup et al., 2010). CSPGs are a family of extracellular matrix molecules up-regulated in the spinal cord after SCI (Jones et al., 2003; Shields et al., 2008). Up-regulation of CSPGs in central nervous system injury inhibits axonal regeneration (Hynds and Snow, 1999; Properzi et al., 2003; Silver and Miller, 2004). Thus, astrocytic glial scar forms a physical and chemical barrier to nerve fiber outgrowth (Huang et al., 2009; Yu et al., 2012). CSPGs consist of a core protein containing one or more unbranched polysaccharide glycosaminoglycan (GAG) chains which contribute to their inhibitory actions (Yu et al., 2012). Many studies have reported that glial scar can be inhibited by chondroitinase ABC (ChABC), an enzyme that selectively cleaves GAG chains from the protein core (Bradbury et al., 2002; Silver and Miller, 2004). Monnier et al. demonstrated that CSPG-associated inhibition of neurite outgrowth is mediated by the Rho/ROCK signaling pathway (Monnier et al., 2003). Coles et al. reported that CSPGs inhibited nerve regeneration through inhibition of receptor protein tyrosine phosphatase sigma (RPTPσ) ectodomain oligomerization (Coles et al., 2011). In this study, we observed that deletion of *LINGO-1* inhibited the formation of glial scar through down-regulation of GFAP and CSPGs after SCI, and promoted regeneration of nerve fibers in the SCI site, providing a source for ascending nerve fibers. The mechanism of reduction of glial scar in response to *LINGO-1* deletion has not been characterized, but it may decrease GFAP expression by acting on its promoter through methylation and deacetylation (Kumar et al., 2018). In addition, regeneration of nerve fibers containing NF and CGRP in the injury site may have originated from the surviving neurons after SCI. We suspect that more neurons had survived in the SCI, resulting in more regenerating nerve fibers in the lesion site and adjacent areas.

5. Conclusions

We observed that the *LINGO-1* KO mice exhibited a lower incidence of cells undergoing apoptosis, decreased inflammation, and reduced glial scar formation, resulting in increased nerve fiber regeneration after SCI when compared with *LINGO-1*$^{+/+}$ mice. These results suggested that *LINGO-1* deletion represents a novel approach to promote axonal regeneration. This may have been a result of reduction of cell apoptosis and improvement of the injury microenvironment through decreased inflammation and glial scar formation in the injured spinal cord. Therefore, inhibition of LINGO-1 may be a promising strategy for treatment of SCI to enhance cell survival and nerve regeneration.

6. Compliance with ethical standards

The use and care of animals were approved by the Ethics Committee of Sun Yat-sen University and carried out in strict accordance with the recommendations in the Guide for the Care and Use of Laboratory Animals of the National Institutes of Health.

Conflict of interests

The authors declare no conflict of interest.

Acknowledgements

The authors thank Ms. Hui Li and Ms. Sai-fei Gao from Guangdong Research Center for Disease-Model Animals, SUN Yat-sen University for designing the *LINGO-1* knockout mice. This research was supported by grants from Co-innovation Foundation of Guangzhou City (201704020221), Chinese National Natural Science Foundation (81330028, 8167150879), Foundation of the Education Ministry of China (201300193035) and Foundation of Guangdong Province (2017B020210012) to Y.S. Zeng, and grants from Start-up Fundation of Guangdong Province (2018A030310113) to G. Li.

Appendix A. Supplementary data

Supplementary data to this article can be found online at https://doi.org/10.1016/j.expneurol.2019.112965.

References

Anderson, M.A., Burda, J.E., Ren, Y., Ao, Y., O'Shea, T.M., Kawaguchi, R., Coppola, G., Khakh, B.S., Deming, T.J., Sofroniew, M.V., 2016. Astrocyte scar formation aids central nervous system axon regeneration. Nature 532, 195–200.

Andrews, J.L., Fernandez-Enright, F., 2015. A decade from discovery to therapy: Lingo-1, the dark horse in neurological and psychiatric disorders. Neurosci. Biobehav. Rev. 56, 97–114.

Beattie, M.S., Farooqui, A.A., Bresnahan, J.C., 2000. Review of current evidence for apoptosis after spinal cord injury. J. Neurotrauma 17, 915–925.

Bianchi, M.E., 2007. DAMPs, PAMPs and alarmins: all we need to know about danger. J. Leukoc. Biol. 81, 1–5.

Bradbury, E.J., Moon, L.D., Popat, R.J., King, V.R., Bennett, G.S., Patel, P.N., Fawcett, J.W., McMahon, S.B., 2002. Chondroitinase ABC promotes functional recovery after spinal cord injury. Nature 416, 636–640.

Capecchi, M.R., 2005. Gene targeting in mice functional analysis of the mammalian genome for the twentyfirst century. Nat. Rev. Genet. 6, 507–512.

Carim-Todd, L., Escarceller, M., Estivill, X., Sumoy, L., 2003. LRRN6A LERN1 leucine-rich repeat neuronal protein 1, a novel gene with enriched expression in limbic system and neocortex. Eur. J. Neurosci. 18, 3167–3182.

Chen, Y., Cao, J., Xiong, M., Petersen, A.J., Dong, Y., Tao, Y., Huang, C.T., Du, Z., Zhang, S.C., 2015. Engineering human stem cell lines with inducible gene knockout using CRISPR/Cas9. Cell Stem Cell 17, 233–244.

Cheriyan, T., Ryan, D.J., Weinreb, J.H., Cheriyan, J., Paul, J.C., Lafage, V., Kirsch, T., Errico, T.J., 2014. Spinal cord injury models: a review. Spinal Cord 52, 588–595.

Coles, C.H., Shen, Y., Tenney, A.P., Siebold, C., Sutton, G.C., Lu, W., Gallagher, J.T., Jones, E.Y., Flanagan, J.G., Aricescu, A.R., 2011. Proteoglycan-specific molecular switch for RPTPsigma clustering and neuronal extension. Science 332, 484–488.

Cong, L., Ran, F.A., Cox, D., Lin, S., Barretto, R., Habib, N., Hsu, P.D., Wu, X., Jiang, W., Marraffini, L.A., Zhang, F., 2013. Multiplex genome engineering using CRISPR/Cas systems. Science 339, 819–823.

Crowe, M.J., Bresnahan, J.C., Shuman, S.L., Masters, J.N., Beattie, M.S., 1997. Apoptosis and delayed degeneration after spinal cord injury in rats and monkeys. Nat. Med. 3, 73–76.

Davalos, D., Grutzendler, J., Yang, G., Kim, J.V., Zuo, Y., Jung, S., Littman, D.R., Dustin, M.L., Gan, W.B., 2005. ATP mediates rapid microglial response to local brain injury in vivo. Nat. Neurosci. 8, 752–758.

David, S., Lopez-Vales, R., Wee Yong, V., 2012. Harmful and beneficial effects of inflammation after spinal cord injury: potential therapeutic implications. Handb. Clin. Neurol. 109, 485–502.

Foale, S., Berry, M., Logan, A., Fulton, D., Ahmed, Z., 2017. LINGO-1 and AMIGO3, potential therapeutic targets for neurological and dysmyelinating disorders. Neural Regen. Res. 12, 1247–1251.

Fu, Q.L., Li, X., Yip, H.K., Shao, Z., Wu, W., Mi, S., So, K.F., 2009. Combined effect of brain-derived neurotrophic factor and LINGO-1 fusion protein on long-term survival of retinal ganglion cells in chronic glaucoma. Neuroscience 162, 375–382.

Fu, Q.L., Hu, B., Li, X., Shao, Z., Shi, J.B., Wu, W., So, K.F., Mi, S., 2010. LINGO-1 negatively regulates TrkB phosphorylation after ocular hypertension. Eur. J. Neurosci. 31, 1091–1097.

Gadani, S.P., Walsh, J.T., Smirnov, I., Zheng, J., Kipnis, J., 2015. The glia-derived alarmin IL-33 orchestrates the immune response and promotes recovery following CNS injury. Neuron 85, 703–709.

Guo, J.S., Zeng, Y.S., Li, H.B., Huang, W.L., Liu, R.Y., Li, X.B., Ding, Y., Wu, L.Z., Cai, D.Z., 2007. Cotransplant of neural stem cells and NT-3 gene modified Schwann cells promote the recovery of transected spinal cord injury. Spinal Cord 45, 15–24.

Gwak, Y.S., Hulsebosch, C.E., 2009. Remote astrocytic and microglial activation modulates neuronal hyperexcitability and below-level neuropathic pain after spinal injury in rat. Neuroscience 161, 895–903.

Hines, D.J., Hines, R.M., Mulligan, S.J., Macvicar, B.A., 2009. Microglia processes block the spread of damage in the brain and require functional chloride channels. Glia 57, 1610–1618.

Huang, X., Kim, J.M., Kong, T.H., Park, S.R., Ha, Y., Kim, M.H., Park, H., Yoon, S.H., Park, H.C., Park, J.O., Min, B.H., Choi, B.H., 2009. GM-CSF inhibits glial scar formation and shows long-term protective effect after spinal cord injury. J. Neurol. Sci. 277, 87–97.

Huang, L.J., Zhang, T., Li, S., Duan, J.T., Ye, F., Li, H.X., She, Z.G., Gao, G.Q., Yang, X., 2014. Anthraquinone G503 induces apoptosis in gastric cancer cells through the mitochondrial pathway. PLoS One 9, 1–13.

Hynds, D.L., Snow, D.M., 1999. Neurite outgrowth inhibition by chondroitin sulfate proteoglycan: stalling/stopping exceeds turning in human neuroblastoma growth cones. Exp. Neurol. 160, 244–255.

Inoue, H., Lin, L., Lee, X., Shao, Z., Mendes, S., Snodgrass-Belt, P., Sweigard, H., Engber, T., Pepinsky, B., Yang, L., Beal, M.F., Mi, S., Isacson, O., 2007. Inhibition of the leucine-rich repeat protein LINGO-1 enhances survival, structure, and function of dopaminergic neurons in Parkinson's disease models. Proc. Natl. Acad. Sci. U. S. A. 104, 14430–14435.

Ito, D., Imai, Y., Ohsawa, K., Nakajima, K., Fukuuchi, Y., Kohsaka, S., 1998. Microglia-specific localisation of a novel calcium binding protein, Iba1. Brain Res. Mol. Brain Res. 57, 1–9.

Ji, B., Li, M., Wu, W.T., Yick, L.W., Lee, X., Shao, Z., Wang, J., So, K.F., McCoy, J.M., Pepinsky, R.B., Mi, S., Relton, J.K., 2006. LINGO-1 antagonist promotes functional recovery and axonal sprouting after spinal cord injury. Mol. Cell. Neurosci. 33, 311–320.

Jo, M.-J., Kumar, H., Joshi, H.P., Choi, H., Ko, W.-K., Kim, J.M., Hwang, S.S.S., Park, S.Y., Sohn, S., Bello, A.B., Kim, K.-T., Lee, S.-H., Zeng, X., Han, I., 2018. Oral administration of α-Asarone promotes functional recovery in rats with spinal cord injury. Front. Pharmacol. 9, 1–11.

Jones, L.L., Margolis, R.U., Tuszynski, M.H., 2003. The chondroitin sulfate proteoglycans neurocan, brevican, phosphacan, and versican are differentially regulated following spinal cord injury. Exp. Neurol. 182, 399–411.

Kigerl, K.A., Gensel, J.C., Ankeny, D.P., Alexander, J.K., Donnelly, D.J., Popovich, P.G., 2009. Identification of two distinct macrophage subsets with divergent effects causing either neurotoxicity or regeneration in the injured mouse spinal cord. J. Neurosci. 29, 13435–13444.

Kono, H., Rock, K.L., 2008. How dying cells alert the immune system to danger. Nat. Rev. Immunol. 8, 279–289.

Kumar, P., Godbole, N.M., Chaturvedi, C.P., Singh, R.S., George, N., Upadhyay, A., Anjum, B., Godbole, M.M., Sinha, R.A., 2018. Mechanisms involved in epigenetic down-regulation of Gfap under maternal hypothyroidism. Biochem. Biophys. Res. Commun. 502, 375–381.

Lai, B.Q., Wang, J.M., Duan, J.J., Chen, Y.F., Gu, H.Y., Ling, E.A., Wu, J.L., Zeng, Y.S., 2013. The integration of NSC-derived and host neural networks after rat spinal cord transection. Biomaterials 34, 2888–2901.

Li, G.L., Brodin, G., Farooque, M., Funa, K., Holtz, A., Wang, W.L., Olsson, Y., 1996. Apoptosis and expression of Bcl-2 after compression trauma to rat spinal cord. J. Neuropathol. Exp. Neurol. 55, 280–289.

Li, X., Liu, D., Xiao, Z., Zhao, Y., Han, S., Chen, B., Dai, J., 2019. Scaffold-facilitated locomotor improvement post complete spinal cord injury: motor axon regeneration versus endogenous neuronal relay formation. Biomaterials 197, 20–31.

Losey, P., Young, C., Krimholtz, E., Bordet, R., Anthony, D.C., 2014. The role of hemorrhage following spinal-cord injury. Brain Res. 1569, 9–18.

Lu, X., Perera, T.H., Aria, A.B., Callahan, L.A.S., 2018. Polyethylene glycol in spinal cord injury repair: a critical review. J. Exp. Pharmacol. 10, 37–49.

McKeon, R.J., Schreiber, R.C., Rudge, J.S., Silver, J., 1991. Reduction of neurite outgrowth in a model of glial scarring following CNS injury is correlated with the expression of inhibitory molecules on reactive astrocytes. J. Neurosci. 11, 3398–3411.

Meabon, J.S., de Laat, R., Ieguchi, K., Serbzhinsky, D., Hudson, M.P., Huber, B.R., Wiley, J.C., Bothwell, M., 2016. Intracellular LINGO-1 negatively regulates Trk neurotrophin receptor signaling. Mol. Cell. Neurosci. 70, 1–10.

Mi, S., Lee, X., Shao, Z., Thill, G., Ji, B., Relton, J., Levesque, M., Allaire, N., Perrin, S., Sands, B., Crowell, T., Cate, R.L., McCoy, J.M., Pepinsky, R.B., 2004. LINGO-1 is a component of the Nogo-66 receptor/p75 signaling complex. Nat. Neurosci. 7, 221–228.

Mi, S., Miller, R.H., Lee, X., Scott, M.L., Shulag-Morskaya, S., Shao, Z., Chang, J., Thill, G., Levesque, M., Zhang, M., Hession, C., Sah, D., Trapp, B., He, Z., Jung, V., McCoy, J.M., Pepinsky, R.B., 2005. LINGO-1 negatively regulates myelination by oligodendrocytes. Nat. Neurosci. 8, 745–751.

Mi, S., Hu, B., Hahm, K., Luo, Y., Kam Hui, E.S., Yuan, Q., Wong, W.M., Wang, L., Su, H., Chu, T.H., Guo, J., Zhang, W., So, K.F., Pepinsky, B., Shao, Z., Graff, C., Garber, E., Jung, V., Wu, E.X., Wu, W., 2007. LINGO-1 antagonist promotes spinal cord remyelination and axonal integrity in MOG-induced experimental autoimmune encephalomyelitis. Nat. Med. 13, 1228–1233.

Mizuno, Y., Mochizuki, H., Sugita, Y., Goto, K., 1998. Apoptosis in neurodegenerative disorders. Intern. Med. 37, 192–193.

Monnier, P.P., Sierra, A., Schwab, J.M., Henke-Fahle, S., Mueller, B.K., 2003. The Rho ROCK pathway mediates neurite growth-inhibitory activity associated with the chondroitin sulfate proteoglycans of the CNS glial scar. Mol. Cell. Neurosci. 22, 319–330.

Ohsawa, K., Imai, Y., Kanazawa, H., Sasaki, Y., Kohsaka, S., 2000. Involvement of Iba1 in membrane ruffling and phagocytosis of macrophages microglia. J. Cell Sci. 113, 3073–3084.

Orr, M.B., Gensel, J.C., 2018. Spinal cord injury scarring and inflammation: therapies targeting glial and inflammatory responses. Neurotherapeutics 15, 541–553.

Platt, R.J., Chen, S., Zhou, Y., Yim, M.J., Swiech, L., Kempton, H.R., Dahlman, J.E., Parnas, O., Eisenhaure, T.M., Jovanovic, M., Graham, D.B., Jhunjhunwala, S.,

Heidenreich, M., Xavier, R.J., Langer, R., Anderson, D.G., Hacohen, N., Regev, A., Feng, G., Sharp, P.A., Zhang, F., 2014. CRISPR-Cas9 knockin mice for genome editing and cancer modeling. Cell 159, 440–455.
Properzi, F., Asher, R.A., Fawcett, J., 2003. Chondroitin sulphate proteoglycans in the central nervous system changes and synthesis after injury. Biochem. Soc. Trans. 31, 335–336.
Ran, F.A., Hsu, P.D., Wright, J., Agarwala, V., Scott, D.A., Zhang, F., 2013. Genome engineering using the CRISPR-Cas9 system. Nat. Protoc. 8, 2281–2308.
Ren, H., Chen, X., Tian, M., Zhou, J., Ouyang, H., Zhang, Z., 2018. Regulation of inflammatory cytokines for spinal cord injury repair through local delivery of therapeutic agents. Adv. Sci. 1800529, 1–16.
Rhodes, K.E., Fawcett, J.W., 2004. Chondroitin sulphate proteoglycans preventing plasticity or protecting the CNS. J. Anat. 204, 33–48.
Ruggieri, S., Tortorella, C., Gasperini, C., 2017. Anti lingo 1 (opicinumab) a new monoclonal antibody tested in relapsing remitting multiple sclerosis. Expert. Rev. Neurother. 17, 1081–1089.
Schachtrup, C., Ryu, J.K., Helmrick, M.J., Vagena, E., Galanakis, D.K., Degen, J.L., Margolis, R.U., Akassoglou, K., 2010. Fibrinogen triggers astrocyte scar formation by promoting the availability of active TGF-beta after vascular damage. J. Neurosci. 30, 5843–5854.
Shields, L.B., Zhang, Y.P., Burke, D.A., Gray, R., Shields, C.B., 2008. Benefit of Chondroitinase ABC on sensory axon regeneration in a laceration model of spinal cord injury in the rat. Surg. Neurol. 69, 568–577.
Shuman, S.L., Bresnahan, J.C., Beattie, M.S., 1997. Apoptosis of microglia and oligodendrocytes after spinal cord contusion in rats. J. Neurosci. Res. 50, 798–808.
Silver, J., Miller, J.H., 2004. Regeneration beyond the glial scar. Nat. Rev. Neurosci. 5, 146–156.
Theotokis, P., Touloumi, O., Lagoudaki, R., Nousiopoulou, E., Kesidou, E., Siafis, S., Tselios, T., Lourbopoulos, A., Karacostas, D., Grigoriadis, N., Simeonidou, C., 2016. Nogo receptor complex expression dynamics in the inflammatory foci of central nervous system experimental autoimmune demyelination. J. Neuroinflammation 13, 265.
Tran, A.P., Warren, P.M., Silver, J., 2018. The biology of regeneration failure and success after spinal cord injury. Physiol. Rev. 98, 881–917.
Ughrin, Y.M., Chen, Z.J., Levine, J.M., 2003. Multiple regions of the NG2 proteoglycan inhibit neurite growth and induce growth cone collapse. J. Neurosci. 23, 175–186.
Wang, H., Yang, H., Shivalila, C.S., Dawlaty, M.M., Cheng, A.W., Zhang, F., Jaenisch, R., 2013. One-step generation of mice carrying mutations in multiple genes by CRISPR/Cas-mediated genome engineering. Cell 153, 910–918.
Wang, X., Cao, K., Sun, X., Chen, Y., Duan, Z., Sun, L., Guo, L., Bai, P., Sun, D., Fan, J., He, X., Young, W., Ren, Y., 2015. Macrophages in spinal cord injury: phenotypic and functional change from exposure to myelin debris. Glia 63, 635–651.
Wanner, I.B., Anderson, M.A., Song, B., Levine, J., Fernandez, A., Gray-Thompson, Z., Ao, Y., Sofroniew, M.V., 2013. Glial scar borders are formed by newly proliferated, elongated astrocytes that interact to corral inflammatory and fibrotic cells via STAT3-dependent mechanisms after spinal cord injury. J. Neurosci. 33, 12870–12886.
Weiner, H.L., 2008. A shift from adaptive to innate immunity: a potential mechanism of disease progression in multiple sclerosis. J. Neurol. 255 (Suppl. 1), 3–11.
Wu, D., Miyamoto, O., Shibuya, S., Okada, M., Igawa, H., Janjua, N.A., Norimatsu, H., Itano, T., 2005. Different expression of macrophages and microglia in rat spinal cord contusion injury model at morphological and regional levels. Acta Med. Okayama 59, 121–127.
Wu, H.F., Cen, J.S., Zhong, Q., Chen, L., Wang, J., Deng, D.Y., Wan, Y., 2013. The promotion of functional recovery and nerve regeneration after spinal cord injury by lentiviral vectors encoding Lingo-1 shRNA delivered by Pluronic F-127. Biomaterials 34, 1686–1700.
Yang, H., Wang, H., Jaenisch, R., 2014. Generating genetically modified mice using CRISPR/Cas-mediated genome engineering. Nat. Protoc. 9, 1956–1968.
Yiu, G., He, Z., 2006. Glial inhibition of CNS axon regeneration. Nat. Rev. Neurosci. 7, 617–627.
Yu, P., Wang, H., Katagiri, Y., Geller, H.M., 2012. An in vitro model of reactive astrogliosis and its effect on neuronal growth. Methods Mol. Biol. 814, 327–340.
Zeng, Y.S., Ding, Y., Wu, L.Z., Guo, J.S., Li, H.B., Wong, W.M., Wu, W.T., 2005. Co-transplantation of schwann cells promotes the survival and differentiation of neural stem cells transplanted into the injured spinal cord. Dev. Neurosci. 27, 20–26.
Zhang, Z., Xu, X., Xiang, Z., Yu, Z., Feng, J., He, C., 2013. LINGO-1 receptor promotes neuronal apoptosis by inhibiting WNK3 kinase activity. J. Biol. Chem. 288, 12152–12160.